

Interstitial-Boron Solution Strengthened WB_{3+x}

Xiyue Cheng¹, Wei Zhang^{1,2}, Xing-Qiu Chen^{1,*}, Haiyang Niu¹, Peitao Liu¹, Kui Du^{1,2,†}, Gang Liu¹, Dianzhong Li¹, Hui-Ming Cheng¹, Hengqiang Ye¹, and Yiyi Li¹

¹ *Shenyang National Laboratory for Materials Science, Institute of Metal Research, Chinese Academy of Sciences, Shenyang 110016, China and*

² *Beijing National Center for Electron Microscopy, Tsinghua University, Beijing 100084, China*
(Dated: February 26, 2022)

By means of variable-composition evolutionary algorithm coupled with density functional theory and in combination with aberration-corrected high-resolution transmission electron microscopy experiments, we have studied and characterized the composition, structure and hardness properties of WB_{3+x} ($x < 0.5$). We provide robust evidence for the occurrence of stoichiometric WB_3 and non-stoichiometric WB_{3+x} both crystallizing in the metastable $hP16$ ($P6_3/mmc$) structure. No signs for the formation of the highly debated WB_4 (both $hP20$ and $hP10$) phases were found. Our results rationalize the seemingly contradictory high-pressure experimental findings and suggest that the interstitial boron atom is located in the tungsten layer and vertically interconnect with four boron atoms, thus forming a typical three-center boron net with the upper and lower boron layers in a three-dimensional covalent network, which thereby strengthen the hardness.

PACS numbers: 71.20.Lp, 71.23.Ft, 76.60.-k, 61.43.Bn

Typical ultrahard or superhard materials [1–3] (i.e., diamond, $c\text{-B}_2\text{CN}$, $c\text{-BN}$, $\gamma\text{-B}_{28}$ [4, 5] and most recently synthesized nanotwinned $c\text{-BN}$ [6]) would require three-dimensional (3D) bonding networks commonly consisting of high densities of strong covalent bonds, atomic constituents and valence electrons as well as nano-scale grains. Currently, the most powerful way to yield the high densities of these factors is the synthesis under high pressure conditions. However, in recent years transition metal borides (OsB_2 , ReB_2 , CrB_4 , and FeB_4 , etc [7–15]) have attracted extensive interests because of superior mechanical properties and ambient-condition synthesis without the need of high pressure, although their hardness is not as hard as superhardness.

Among those borides, the W-B system has attracted particular attention since the report [16] on WB_4 with a measured superhardness, H_v of about 46.3 GPa, under the loading force of 0.49 N, as the highest measured hardness among those borides mentioned above. Although the superhardness of WB_4 has been again confirmed experimentally [17] and interpreted theoretically [18] based on the widely accepted $hP20\text{-WB}_4$ structure [16, 17, 19, 20], several subsequent first-principles calculations denied its existence [21–23]. This structure is neither thermodynamically [21] nor dynamically [22] stable, and also not superhard [24] ($H_v = 6.5$ GPa according to a recently proposed hardness model [25, 26]). Instead, those first-principles calculations [21–23] suggested that the experimentally attributed WB_4 [17, 27, 28] should be characterized as a $hP16\text{-WB}_3$ phase.

Given the fact that the theoretically proposed $hP16\text{-WB}_3$ [21–23] is thermodynamically and mechanically stable, and its XRD pattern matches well the experimentally observed ones [17, 19], there seems no reason to suspect the reliability of its composition and structure. However, it is highly surprising that four recent high-pressure ex-

perimental findings of this phase [16, 28–30] yielded conflicting tendency of the pressure dependence normalized c/a ratio. The more striking fact is that none of them agrees with the theoretically derived pressure-dependent c/a ratio [31] of $hP16\text{-WB}_3$. Therefore, this tungsten boride still needs further clarification.

Within this context, by combining first-principles calculations [32, 33] (unless otherwise mentioned, all calculations have been performed with the Perdew-Burke-Ernzerh generalized gradient approximation (GGA-type PBE) [34]), variable-composition evolutionary algorithm search as implemented recently in USPEX [35, 36] and the aberration-corrected images of high resolution transmission electron microscopy (Ac-HRTEM) (method details refers to Supporting information), we have confirmed the existence of WB_{3+x} ($x < 0.5$) (including the stoichiometric $hP16\text{-WB}_3$) and denied the formation of the extensively debated boride of $hP20\text{-WB}_4$ [17, 27, 28]. The previously experimentally attributed WB_4 is indeed WB_{3+x} . The results uncovered that the structure can be regarded as a defective $hP16\text{-WB}_3$ one but with a certain proportion x of extra interstitial boron locating in the tungsten atomic layers. Varying x , the normalized c/a ratio rationalized four puzzling high-pressure experimental findings [16, 28–30]. Importantly, our results revealed that the interstitial boron solution highlights an effect of strengthening (hardening) to the mechanical property of WB_{3+x} because of the appearance of the 3D covalent framework induced by boron solution from the ideal 2D boron sheets in $hP16\text{-WB}_3$.

The USPEX searched results are compiled in Fig. 1 (details refer to Supporting information and Figure S1). Although the USPEX found a lowest-enthalpy $hP10\text{-WB}_4$ (MoB_4 -type, Fig. 1(c)) in accordance with four recently theoretical results [14, 23, 37, 38], its enthalpy of formation lies about 2.3 meV/atom above the $hR24\text{-WB}_3$

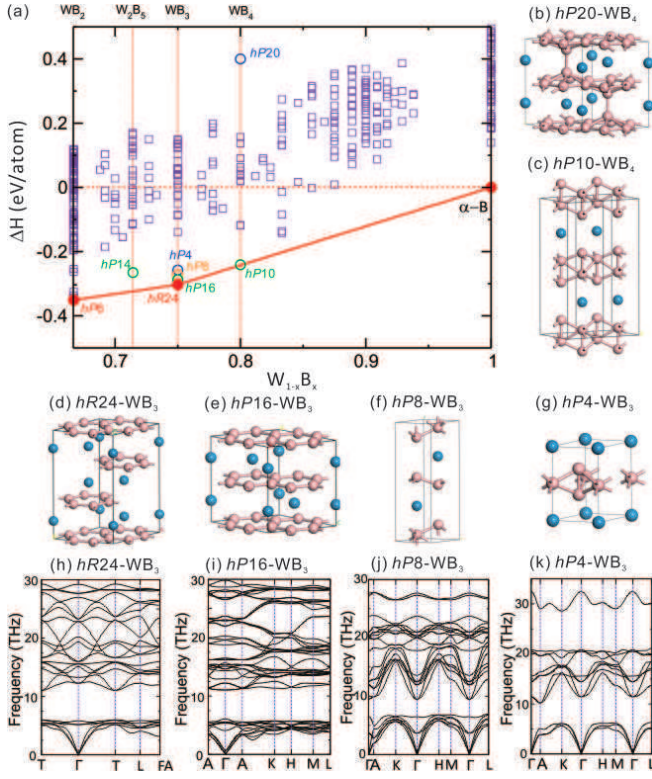


FIG. 1: (color online) (a) The derived GGA-type PBE enthalpies of formation predicted by variable-composition evolutionary computations for the WB_2 -B system (more details refer to Supporting information). Every square represents an individual structure and the most stable ground state phases (solid circles) are connected to a convex hull. Hollow circles denote metastable phases above the convex hull. In panels (b) and (c), the crystal structures of WB_4 : (b) the previously experimental attributed structure ($hP20$) and (c) the USPEX searched ground state phase ($hP10$); In panels (d) to (k), the USPEX searched crystal structures and their corresponding phonon dispersions of WB_3 : (d,h) $hR24$, (e,i) $hP16$, (f,j) $hP8$, and (g,k) $hP4$.

$\leftrightarrow \alpha$ -B tieline of the convex hull, suggesting its instability at $T = 0$ K. In addition, the experimentally attributed $hP20$ - WB_4 phase (Fig. 1(b)) is confirmed to be definitely unstable because its enthalpy is positive, much higher than the convex hull. Therefore, we excluded the existence of WB_4 at the ground state. At WB_3 composition, the USPEX searches demonstrated that the stability of WB_3 is highly robust at the ground state (Fig. 1(a)). The results suggest that WB_3 has a lowest-enthalpy $hR24$ ($R\bar{3}m$) structure agreeing with the recent results [23, 38] and has three metastable phases (Fig. 1(d - g)), $hP16$ ($P6_3/mmc$) [21–23], $hP8$ ($P\bar{3}m1$), and $hP4$ ($P\bar{6}m2$) with little energy deviations. Their optimized lattice parameters are compiled in supporting information, Table S3. These four lattices have been confirmed dynamically stable by the derived phonon dispersions without any imaginary frequencies, as illustrated

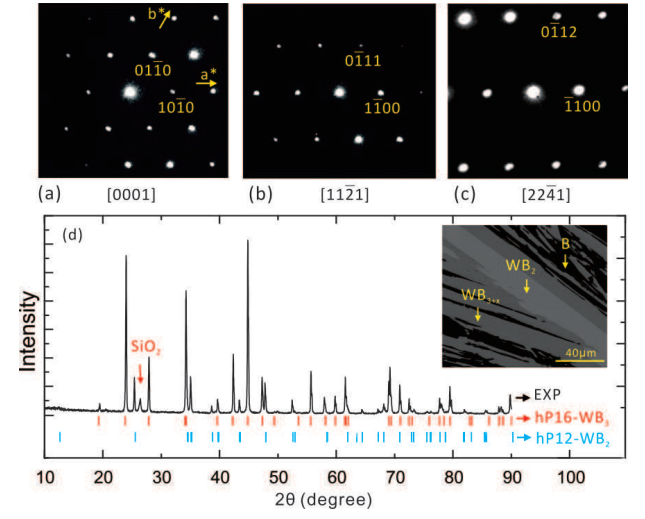


FIG. 2: (color online) (a-c) Experimental electron diffraction (ED) patterns along the $[10\bar{1}0]$, $[11\bar{2}1]$ and $[22\bar{4}1]$ directions, respectively. (d) The experimental X-ray diffraction data; reflections of the ideal $hP16$ - WB_3 and $hP12$ - WB_2 are indicated by vertical bars. Right inset in (d) shows an SEM image of annealed sample. Note that amorphous boron could not be distinguished by the XRD pattern. Besides, the 26.4° peak origins from SiO_2 which was ground by the much harder WB_{3+x} in the preparation of the x-ray diffraction powder using an agate mortar and pestle.

in Fig. 1(j - m). From the phonon densities of states, we further derived the temperature-dependent Gibbs free energies by also including zero-point energies and static DFT energies among these phases (Fig. 1(c)), revealing a phase transition from the ground state $hR24$ - WB_3 to the metastable $hP16$ - WB_3 phase above 659 K. In order to elucidate the impact of the exchange-correlation functional on phase transition, we further employed the localized density approximation (LDA) potential [39] and found consistently this phase transition above 678 K (Supporting information, Figure S2).

To clarify these theoretical results, we further measured XRD patterns of the powder sample annealed for 144 hours at 1523 K (details refer to Supporting information). As illustrated in Fig. 2(d), the XRD pattern uncovers the mixture of WB_2 and WB_{3+x} . Furthermore, from the SEM image (see, insert of Fig. 2d), the dendrite of WB_2 and WB_{3+x} can be identified, whereas the dark contrasting part is amorphous boron which can not be detectable by XRD. It is clear that the XRD pattern of WB_2 indicates a $hP12$ (WB_2 -type) phase, in good agreement with the previous experimental characterization [10]. The XRD pattern of WB_{3+x} has been found in accordance with the reported ones [17, 27, 28] and is exactly same with the theoretically proposed metastable $hP16$ - WB_3 phase, rather than its ground state $hR24$ - WB_3 phase. This fact can be interpreted well, since our

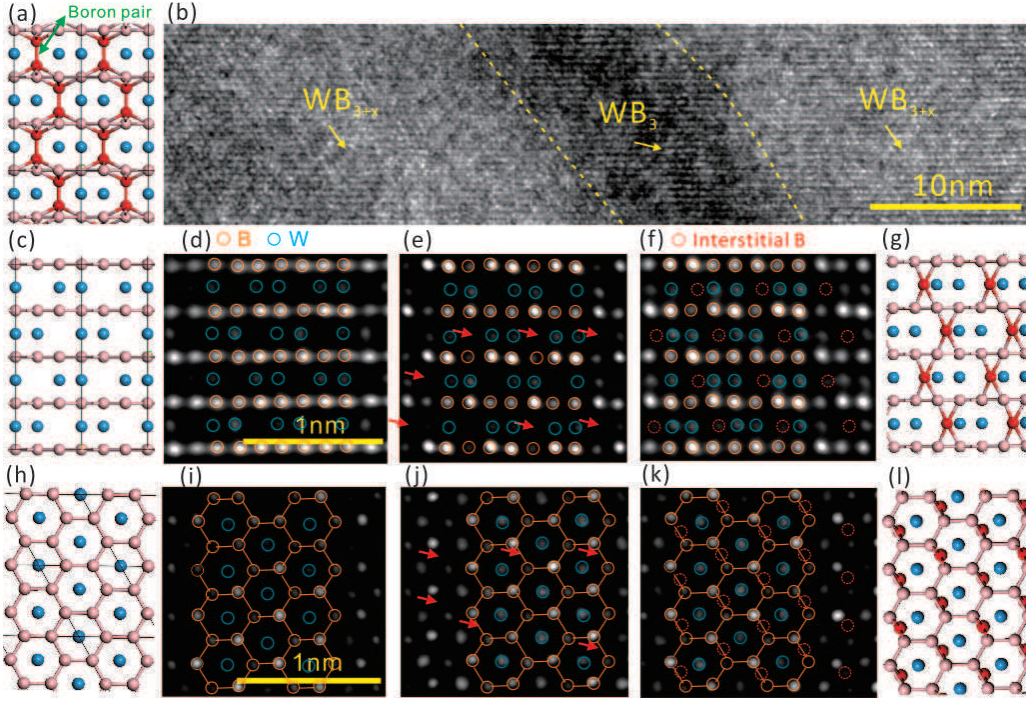


FIG. 3: (color online) The Ac-HRTEM characterization of the superhard WB_{3+x} . (a) The projection along the $[11\bar{2}0]$ direction of the $hP20-WB_4$ [16, 17, 27, 28]. (b) The Ac-HRTEM morphology with a 10 nm dimension. (c) and (h) The projections along the $[11\bar{2}0]$ and $[0001]$ directions of $hP16-WB_3$, respectively. (d,e,f) and (i,j,k) The Ac-HRTEM images with the 1 nm dimension projected along the $[11\bar{2}0]$ and $[0001]$ directions of defective WB_{3+x} , respectively. (g and l) the projections of the structural model along the $[11\bar{2}0]$ and $[0001]$ directions of defective WB_{3+x} , respectively.

annealed temperature of 1523 K is much higher than our estimated temperature (659 K (GGA) and 678 K (LDA)) of phase transition (Fig. 1(c)). Furthermore, the electron diffraction ED images (Fig. 2(a-c)) and the XRD pattern (Fig. 2d) evidence a hexagonal structure of WB_{3+x} with the lattice parameters of $a = 5.2055 \text{ \AA}$, $c = 6.3348 \text{ \AA}$ and the axial ratio $c/a = 1.2169$, agreeing well with the previously reported data [17, 27, 28]. Moreover, the Vickers hardness of the polycrystal sample of WB_{3+x} was measured to be 36.7 GPa under a loading force of 1N, which is comparable to the reported values (31.8 GPa under 1.2 N [16] and 38.3 GPa under 1N [17]).

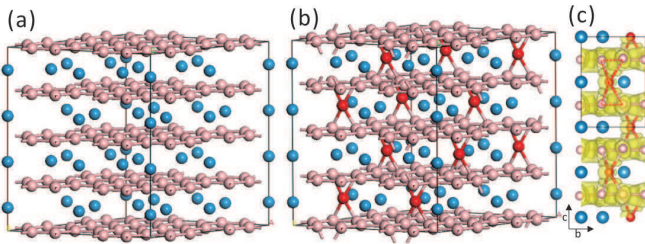


FIG. 4: (color online) The $2 \times 2 \times 2$ supercell of (a) stoichiometric $hP16-WB_3$, (b) non-stoichiometric WB_{3+x} , and (c) the partial isosurface of the ELF (with an isovalue of 0.65) projected along the $[11\bar{2}0]$ of WB_{3+x} , mainly illustrating the three-center covalent boron net as marked by the dashed line.

Because boron is a weak electronic scatterer, it is impossible to refine the accurate structure of WB_{3+x} from XRD patterns of powder samples. However, the Ac-HRTEM image [40] provides a powerful tool to directly

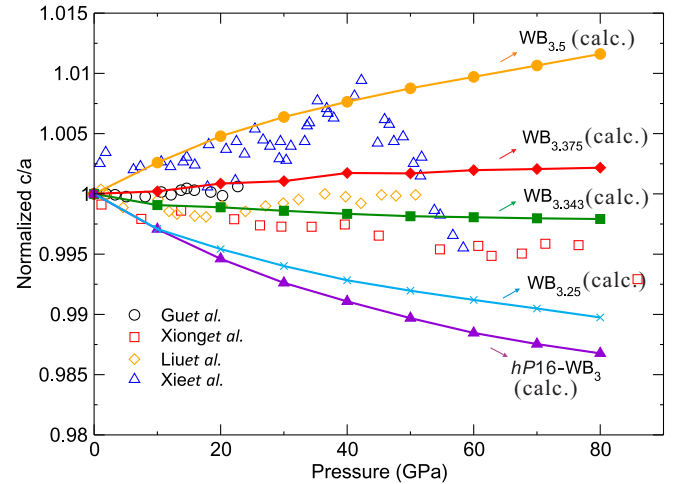


FIG. 5: (color online) The calculated pressure dependence of the normalized c/a ratio of WB_{3+x} ($0 < x < 0.5$), interpreting well the seemingly contradictory experimental results [16, 28–30].

visualize the light mass elements (i.e., oxygen and boron) with the minimum resolution length of about 0.8 \AA (Supporting information). Figure 3b shows the Ac-HRTEM morphology of WB_{3+x} and boundaries between the dark and bright regions can be clearly identified as marked by the dashed curves. The Ac-HRTEM images with the 1nm dimension of Fig. 3(d,e,f) were selected along the $[11\bar{2}0]$ projection, while Fig. 3(i,j,k) corresponds to the same region along the $[0001]$ projection. Interestingly, Fig. 3d and 3i perfectly match the theoretical projec-

tions (Fig. 3c and 3h) along the same directions of the $hP16-WB_3$, confirming the existence of the stoichiometric $hP16-WB_3$. For the $[11\bar{2}0]$ projection of $hP16-WB_3$, between any two dense boron lines there exists a tungsten-atom line, which consists of a repeated unit of every two tungsten atoms separated by a void. However, what out of our expectation is that the voids are partially occupied in the WB_3/WB_{3+x} boundary (see arrows in Fig. 3e) and fully occupied in Fig. 3f (see dashed hollow circles). We further identify that these voids should be occupied by extra boron atoms, rather than tungsten atoms. If the tungsten atom occupies these voids, the extra peaks would be expected to appear from the XRD patterns in Fig. 2d. As further evidence, the extra atoms can be also found in the Ac-HRTEM images in Fig. 3j and 3k projected along the $[0001]$ direction. The fact reflects well the occurrence of the new composition of WB_{3+x} , which shares, accordingly, the same hexagonal structure with the $hP16-WB_3$. In other words, WB_{3+x} can be considered as defective $hP16-WB_3$ in which the extra x boron atoms occupy the interstitial sites in the tungsten layers. Moreover, the previously experimentally attributed $hP20-WB_4$ [17, 27, 28] have been absolutely excluded, because no any boron pairs (as illustrated in Fig. 3a projected along its $[11\bar{2}0]$ direction) can be identified in the Ac-HRTEM images (Fig. 3(d-f)).

We further performed a series of first-principles computational experiments to analyze the exact position of the interstitial boron atoms within a $2 \times 2 \times 2$ supercell of $hP16-WB_3$ (Fig. 4a). According to the Ac-HRTEM images, the interstitial boron atoms are placed in the same layers of tungsten atoms but deviated from all tungsten atoms if viewed from the $[0001]$ direction. After the relaxation, these interstitial boron atoms still locate in the layers of tungsten atoms but now each interstitial boron binds four nearest boron atoms, equivalently, from its upper and lower boron hexagonal rings, as shown in Fig. 4b. These positions nicely agree with our Ac-HRTEM images (Fig. 3f and 3k). In fact, there exists sixteen equivalent interstitial sites in this supercell, determining that the maximum x would be 0.5. To keep the full agreement with the experimental Ac-HRTEM results in Fig. 3f and 3k, at least eight interstitial sites (namely, $WB_{3.25}$) have to be occupied by boron. Therefore, the x content in the boundary region in Fig. 3e and 3j should be below 0.25. Figure 3g and 3l illustrate the projections along the $[11\bar{2}0]$ and $[0001]$ directions for $WB_{3.25}$, in agreement with the Ac-HRTEM images (e.g., Fig 3f and 3k). In addition, it can be seen that the Ac-HRTEM images of WB_{3+x} along $[11\bar{2}0]$ and $[0001]$ directions are well consistent with the simulated images (Supporting information, Figure S3) of the proposed structural model.

Another compelling support to the defective WB_{3+x} is the normalized pressure dependent c/a ratio (Fig. 5). In agreement with the reported results by Zang *et al.* [31], the stoichiometric $hP16-WB_3$ exhibits a large neg-

ative pressure dependence. However, with increasing x , the pressure dependence is substantially elevated. As a result, this behavior interprets well the apparently contradictory results from four recent high pressure measurements. It can be seen that with $x = 0.343$ the theoretical trend is similar to that of the experimental observations [29, 30] whereas with $x = 0.375$ the normalized c/a ratio remains nearly unchanged in the pressure region considered here, which again agrees well with another experimental findings [16]. When x reaches its maximum of 0.5, the normalized c/a ratio rises significantly from 1 to 1.0115 with increasing pressure up to 45 GPa, matching the experimental observation by Xie *et al* [28], although our theoretical trend does not reproduce the experimentally observed quick drop by less than 1 from 45 GPa to 60 GPa.

Mechanically, upon different conditions (temperature and pressure) of synthesis a certain proportion of interstitial boron atom diffuses in the space featured by any two ideal 2D boron sheets (Fig. 4a) in $hP16-WB_3$. This kind of boron solution contributes an extrinsic component to the superhardness and strengths of WB_{3+x} due to the formation of 3D covalent network through the connection of the three-center covalent boron nets as highlighted by dashed lines in Fig. 4c. Our results demonstrated that the interstitial boron atoms in a solid solution way are considered as an efficient routine to tune the mechanical properties (hardness) of transition-metallic borides. The findings highlight a promising factor utilizing the concept of solid solution [27] to design superhard materials, besides our widely recognized manipulations of covalent bonds, valence electrons and atomic constituents as well as nano-scale grains. In addition, despite of a good level of maturity of structural searches for materials discovery, those successful methods (USPEX [35, 36], AIRSS [41], MAISE [42], CALYPSO [23], and AFLOW [15], etc) may need further algorithm implementations on the search of this class of defective or non-stoichiometric structures. Finally, our detailed theoretical and experimental studies of this tungsten boride demonstrate that the compositions and structures of many reportedly known transition metal borides need to be further investigated in-depth using advanced techniques coupled with the art-of-the-state first-principles calculations, in terms of the characterization difficulties of boron atoms.

Acknowledgements We are grateful for the useful discussions with Artem Oganov and Qiang Zhu and for the experimental synthesis with Jiaqi Wang and Shi Liu. This work was supported by the ‘‘Hundred Talents Project’’ of the Chinese Academy of Sciences and from NSFC of China (Grand Numbers: 51074151, 51174188, 51171188) as well as Beijing Supercomputing Center of CAS (including its Shenyang branch) and Vienna Scientific Clusters. This work made use of the resources of the Beijing National Center for Electron Microscopy.

* Corresponding author: xingqiu.chen@imr.ac.cn

† Corresponding author: kuidu@imr.ac.cn

- [1] Kaner, R. B.; Gilman, J. J.; Tolbert, S. H. *Science* **2005**, 308, 1268-1269.
- [2] Brazhkin, V.; Dubrovinskaia, N.; Nicol, M.; Novikov, N.; Riedel, R.; Solozhenko, V.; Zhao, Y. *Nat. Mater.* **2004**, 3, 576-577.
- [3] Gilman, J. J. *Science* **1993**, 261, 1436-1439.
- [4] Oganov, A. R.; Chen, J.; Gatti, C.; Ma, Y.; Glass, C. W.; Liu, Z.; Yu, T.; Kurakevych, O. O.; Solozhenko, V. L. *Nature* **2009**, 457, 863-867.
- [5] Zarechnaya, E.; Dubrovinsky, L.; Dubrovinskaia, N.; Filinchuk, Y.; Chernyshov, D.; Dmitriev, V.; Miyajima, N.; El Goresy, A.; Braun, H.; Van Smaalen, S.; Kantor, I.; Kantor, A.; Prakapenka, V.; Hanfland, M.; Mikhaylushkin, A.; Abrikosov, I.; Simak, S. *Phys. Rev. Lett.* **2009**, 102, 185501.
- [6] Tian, Y.; Xu, B.; Yu, D.; Ma, Y.; Wang, Y.; Jiang, Y.; Hu, W.; Tang, C.; Gao, Y.; Luo, K.; Zhao, Z.; Wang, L. M.; Wen, B.; He, J.; Liu, Z. *Nature* **2013**, 493, 385-388.
- [7] Chung, H. Y.; Weinberger, M. B.; Levine, J. B.; Cumberland, R. W.; Kavner, A.; Yang, J. M.; Tolbert, S. H.; Kaner, R. B. *Science* **2007**, 316, 436-439.
- [8] Levine, J. B.; Nguyen, S. L.; Rasool, H. I.; Wright, J. A.; Brown, S. E.; Kaner, R. B. *J. Am. Chem. Soc.* **2008**, 130, 16953-16958.
- [9] Kolmogorov, A. N.; Shah, S.; Margine, E. R.; Bialon, A. F.; Hammerschmidt, T.; Drautz, R. *Phys. Rev. Lett.* **2010**, 105, 217003.
- [10] Chen, X.-Q.; Fu, C.; Kr?mar, M.; Painter, G. *Phys. Rev. Lett.* **2008**, 100, 19643.
- [11] Levine, J. B.; Tolbert, S. H.; Kaner, R. B. *Adv. Func. Mater.* **2009**, 19, 3519-3533.
- [12] Ivanovskii, A. L. *Progress in Materials Science* **2012**, 57, 184-228.
- [13] Niu, H. Y.; Wang, J. Q.; Chen, X.-Q.; Li, D. Z.; Li, Y. Y.; Lazar, P.; Podlucky, R.; Kolmogorov, A. N. *Phys. Rev. B* **2012**, 85, 144116.
- [14] Gou, H.; Li, Z.; Niu, H.; Gao, F.; Zhang, J.; Ewing, R. C.; Lian, J. *Appl. Phys. Lett.* **2012**, 100, 111907.
- [15] Curtarolo, S.; Hart, G. L. W.; Nardelli, M. B.; Mingo, N.; Sanvito, S.; Levy, O. *Nat. Mater.* **2013**, 12, 191-201.
- [16] Gu, Q. F.; Krauss, G.; Steurer, W. *Adv. Mater.* **2008**, 20, 3620-3626.
- [17] Mohammadi, R.; Lech, A. T.; Xie, M.; Weaver, B. E.; Yeung, M. T.; Tolbert, S. H.; B., K. *Proc. Natl. Acad. Sci. U.S.A.* **2011**, 108, 10958-10962.
- [18] Wang, M.; Li, Y. W.; Cui, T.; Ma, Y. M.; Zou, G. T. *Appl. Phys. Lett.* **2008**, 93, 101905.
- [19] Romans, P. A.; Krug, M. P. *Acta Crystallogr.* **1966**, 20, 313-315.
- [20] Nowotny, H.; Haschke, H.; Benesovsky, F. *Monatsh. Chem.* **1967**, 98, 547-554.
- [21] Liang, Y. C.; Yuan, X.; Zhang, W. Q. *Phys. Rev. B* **2011**, 83, 220102(R).
- [22] Zhang, R.; Legut, D.; Lin, Z.; Zhao, Y.; Mao, H.; Veprek, S. *Phys. Rev. Lett.* **2012**, 108, 255502.
- [23] Li, Q.; Zhou, D.; Zheng, W. T.; Ma, Y. M.; Chen, C. F. *Phys. Rev. Lett.* **2013**, 110, 136403.
- [24] Liang, Y. C.; Fu, Z.; Yuan, X.; Wang, S. M.; Zhong, Z.; Zhang, W. Q. *EPL (Europhysics Letters)* **2012**, 98, 66004.
- [25] Chen, X.-Q.; Niu, H.; Franchini, C.; Li, D.; Li, Y. *Phys. Rev. B* **2011**, 84, 121405.
- [26] Chen, X.-Q.; Niu, H.; Li, D.; Li, Y. *Intermetallics* **2011**, 19, 1275-1281.
- [27] Mohammadi, R.; Xie, M.; Lech, A. T.; Turner, C. L.; Kavner, A.; Tolbert, S. H.; Kaner, R. B. *J. Am. Chem. Soc.* **2012**, 134, 20660-20668.
- [28] Xie, M.; Mohammadi, R.; Mao, Z.; Armentrout, M.; Kavner, A.; Kaner, R.; Tolbert, S. *Phys. Rev. B* **2012**, 85, 064118.
- [29] Xiong, L.; Liu, J.; Bai, L. G.; Li, Y. C.; Lin, C. L.; He, D. W.; Peng, F.; Lin, J.-F. *J. Appl. Phys.* **2013**, 113, 033507.
- [30] Liu, C. J.; Peng, F.; Tan, N.; Liu, J.; Li, F. J.; Qin, J. Q.; Wang, J. H.; Wang, Q. M.; He, D. W. *High Pressure Res.* **2011**, 31, 275-282.
- [31] Zang, C. P.; Sun, H.; Tse, J. S.; Chen, C. F. *Phys. Rev. B* **2012**, 86, 014108.
- [32] Kresse, G.; Hafner, J. *Phys. Rev. B* **1993**, 47, 558-561.
- [33] Kresse, G.; Furthmüller, J. *Phys. Rev. B* **1996**, 54, 11169-11186.
- [34] Perdew, J. P.; Burke, K.; Ernzerhof, M. *Phys. Rev. Lett.* **1996**, 77, 3865.
- [35] Oganov, A. R.; Glass, C. W. *J. Chem. Phys.* **2006**, 124, 244704.
- [36] Oganov, A. R.; Lyakhov, A. O.; Valle, M. *Acc. Chem. Res.* **2011**, 44, 227C237.
- [37] Zhang, M. G.; Yan, H. Y.; Wei, Q.; Wang, H. *Comput. Mat. Sci.* **2013**, 68, 371-378.
- [38] Liang, Y. C.; Gou, Y. P.; Yuan, X.; Zhong, Z.; Zhang, W. Q. *Chem. Phys. Lett.* **2013**, 580, 48-52.
- [39] Perdew, J. P.; Wang, Y. *Phys. Rev. B* **1992**, 45, 13244.
- [40] Jia, C. L.; Lentzen, M.; Urban, K. *Science* **2003**, 299, 870-873.
- [41] Pickard, C. J.; Needs, R. J. *J. Phys. Condens Matter.* **2011**, 23, 053201.
- [42] Kolmogorov, A. N.; Shah, S.; Margine, E. R.; Kleppe, A. K.; Jephcoat, A. P. *Phys. Rev. Lett.* **2012**, 109, 075501.